Journal of Civil Engineering and Urban Planning (2026)
Clausius Scientific Press, Canada

DOI: 10.23977/jceup.2026.080206
ISSN 2616-3969 Vol. 8 Num. 2

Distribution Transformation-Based Method for Simulating Stationary Non-Gaussian Stochastic Processes

Jinyu Zhang*, Xiaowen Ji

Key Laboratory of Urban Security and Disaster Engineering of Ministry of Education, Beijing University of Technology, Beijing 100124, China
**Corresponding Author*

Keywords: Non-Gaussian Stochastic Process; Power Spectrum; Distribution Correlation; Gaussian Process; Spectral Representation

Abstract: Simulation of stationary non-Gaussian stochastic processes with prescribed marginal distributions and second-order dependence structures is important in wind engineering and random vibration analysis. This study proposes a new power-spectrum-based simulation method to jointly represent the marginal distribution and dependence structure. A distribution process is introduced as an intermediate representation, and the distribution correlation of the target non-Gaussian process is transformed into the Pearson correlation of the underlying Gaussian process within the Gaussian copula framework. The corresponding power spectrum is further defined to describe the frequency-domain dependence structure. Based on this formulation, a standard procedure and a simplified procedure are developed. The standard procedure retains the complete correlation transformation, whereas the simplified procedure uses a linear approximation to reduce computational complexity. Numerical examples of single-point non-Gaussian processes and a two-dimensional multi-point inflow wind field show that the proposed method can reproduce the target marginal distributions, power spectral densities, cross-power spectra, and coherence structures. The standard procedure is more stable for multi-point dependence, while the simplified procedure provides an efficient approximation for rapid simulation and large-scale parametric analysis.

1. Introduction

The simulation of stationary stochastic processes is a fundamental issue in structural wind engineering, random vibration, and reliability analysis. For Gaussian stochastic processes, the statistical characteristics can be fully described by the mean, variance, correlation function, or power spectral density. Therefore, the spectral representation method based on prescribed correlation functions or power spectral densities has been well developed and widely applied to one-dimensional processes, multivariate processes, and spatial random fields[1–10]. However, practical engineering loads and structural responses are often not strictly Gaussian. Wind pressures, fluctuating wind velocities, and nonlinear structural responses may exhibit skewness, heavy tails, or sharp peaks, making conventional Gaussian models insufficient for simultaneously representing marginal distributions and dependence structures.

Existing methods for simulating non-Gaussian stochastic processes are mostly based on the translation-process framework. In this framework, an underlying Gaussian process is first generated and then transformed into the target non-Gaussian process through a memoryless nonlinear mapping[11–18]. Hermite polynomial models, Johnson transformations, Gamma-distribution-based transformations, and kernel-density-based transformations are typical examples of this type of method. The translation-process method is attractive because of its clear formulation, convenient implementation, and ability to control the target marginal distribution. It has therefore been widely used in non-Gaussian wind load simulation, fatigue analysis, extreme value estimation, and reliability assessment[13–19].

However, the main challenge of the translation-process method lies in preserving the second-order dependence structure. A nonlinear marginal transformation usually changes the correlation function and power spectral density of the underlying Gaussian process. As a result, the target marginal distribution and the target second-order structure are difficult to satisfy at the same time. To reduce this discrepancy, correlation-function inversion, spectral correction, iterative updating, and higher-order spectral methods have been proposed[20–31]. These methods improve the simulation accuracy of non-Gaussian processes to some extent, but they usually require complicated integrations, numerical iterations, or spectral corrections. In multi-point simulations, the resulting underlying Gaussian cross-spectral matrix may also become unrealizable. Therefore, a more direct way to coordinate non-Gaussian marginal distributions and second-order dependence structures is still needed.

Copula theory provides another perspective for this problem. According to Sklar's theorem, a multivariate joint distribution can be decomposed into marginal distributions and a copula-based dependence structure, which provides a theoretical basis for modeling non-Gaussian dependence[32–38]. Unlike Pearson's linear correlation, Spearman correlation equivalent to measure correlation between distributions mainly measures monotonic correlation and remains invariant under strictly increasing transformations[39–41]. This property makes distribution correlation a suitable intermediate dependence measure between non-Gaussian variables and underlying Gaussian variables. Existing copula and distribution-correlation methods have mainly been developed for finite-dimensional random variables. For stationary stochastic processes, however, distribution correlation has rarely been incorporated into a frequency-domain simulation framework for stationary non-Gaussian stochastic processes.

To address this issue, this study proposes a simulation method for stationary non-Gaussian stochastic processes based on distribution transformation. Within the Gaussian copula framework, a closed-form mapping is first established between the distribution correlation of the target non-Gaussian process and the Pearson correlation of the underlying Gaussian process. Then, a standardized distribution transformation process is constructed, and the power spectrum corresponding to the distribution-correlation function is defined. In this way, the distribution-based dependence structure is extended from the time domain to the frequency domain. Based on this formulation, both a standard simulation procedure and a simplified simulation procedure are developed. Single-point benchmark examples and a two-dimensional multi-point inflow wind field example are used to verify the capability of the proposed method to preserve both marginal distributions and second-order dependence structures.

2. Distribution Transformation

2.1 Second-Order Probabilistic Characteristic Transformation Problem

Let $\mathbf{X}(t)=[X_1(t),X_2(t),...,X_n(t)]^T$ denote an n-dimensional stationary non-Gaussian stochastic vector process. In the translation-process method, an underlying standard Gaussian stochastic vector

process $\mathbf{U}(t)=[\mathrm{U}_1(t),\mathrm{U}_2(t),\ldots,\mathrm{U}_n(t)]^T$ is constructed, and the target non-Gaussian process is then obtained through marginal distribution transformation:

$$X_i(t)=T_i(U_i(t)) \qquad i=1,2,...,n \tag{1}$$

where $T_i(\cdot)$ is the nonlinear transformation function determined by the target marginal distribution. Since $T_i(\cdot)$ is nonlinear, the correlation function of the target non-Gaussian process is not identical to that of the underlying Gaussian process. For an arbitrary time lag τ, the two are related by

$$\begin{aligned} R_{X,ij}(\tau) &= E[T_i(U_i(t))T_j(U_j(t+\tau))] \\ &= \int_{-\infty}^{+\infty}\int_{-\infty}^{+\infty} T_i(u_1)T_j(u_2)\cdot\varphi(u_1,u_2;\rho_{U,ij}(\tau))du_1du_2 \end{aligned} \tag{2}$$

This equation shows that the correlation function of the target non-Gaussian process and that of the underlying Gaussian process are connected through a nonlinear mapping governed by the marginal distribution. When the target correlation function or power spectral density is prescribed, the corresponding underlying Gaussian correlation structure usually has to be obtained through numerical integration and inverse solution. In multi-point stochastic process simulation, this procedure is also constrained by the realizability of the spectral matrix.

2.2 Empirical Distribution Process and Distribution-Correlation Transformation

For the i-th component $X_i(t)$ of the n dimensional stationary non-Gaussian stochastic vector process $\mathbf{X}(t)$, samples are taken at equal time intervals $t_m=m\Delta t$:

$$x_{i,m}=X_i(t_m) \qquad m=1,2,...,M \tag{3}$$

The sequence is sorted in ascending order, and the order of $x_{i,m}$ in the sample set is denoted by $r_{i,m}$. The empirical distribution process is then constructed as

$$D_{i,M}(t_m)=\frac{r_{i,m}}{M+1} \tag{4}$$

For a finite sample, the distribution process can be interpreted as the empirical cumulative distribution function of the sample. As the sample size increases, it gradually approaches the true cumulative distribution function.

For two components $X_i(t)$ and $X_j(t+\tau)$, the distribution correlation can be defined as the Pearson correlation coefficient between the corresponding distribution variables. Since $D_i(t)\sim U(0,1)$, its mean and variance are 1/2 and 1/12, respectively. Then

$$\rho_{ij}^{D}(\tau)=12E(D_i(t)D_j(t+\tau))-3 \tag{5}$$

Within the Gaussian copula framework, let $\rho_{U,ij}^{\text{Pearson}}$ be the Pearson correlation function of the underlying standard Gaussian process $\mathbf{U}(t)$. In the large-sample limit,

$$D_i(t)=F_i(X_i(t))=\Phi(\mathrm{U}_i(t)) \tag{6}$$

where $F_i(\cdot)$ is the marginal distribution function of the i-th component, and $\Phi(\cdot)$ is the standard Gaussian cumulative distribution function. Based on Plackett's identity and further derivation, Eq. (5) can be written as

$$\rho_{ij}^{D}(\tau)=\frac{6}{\pi}\arcsin(\frac{\rho_{U,ij}^{\text{Pearson}}(\tau)}{2}) \tag{7}$$

The inverse transformation is then

$$\rho_{U,ij}^{\text{Pearson}}(\tau)=2\sin(\frac{\pi}{6}\rho_{ij}^{D}(\tau)) \tag{8}$$

This equation establishes a closed-form transformation between the distribution correlation function of the target non-Gaussian process and the Pearson correlation function of the underlying Gaussian process. Compared with the inverse double integration used in the traditional translation method, the distribution-correlation transformation is more direct and concise.

2.3 Construction of Distribution Transformation

Let $\mathbf{X}(t)=[X_1(t),X_2(t),...,X_n(t)]^T$ be a stationary non-Gaussian stochastic vector process. Since the process is stationary, the marginal distribution of the i-th component is independent of time and is denoted by

$$F_i(x)=P\{X_i(t)\le x\} \tag{9}$$

When $F_i(x)$ is continuous, the distribution process can be defined as

$$D_i(t)=F_i(X_i(t)) \qquad D_i(t)\sim U(0,1) \tag{10}$$

Thus, the distribution transformation can be regarded as a quantile mapping induced by the marginal distribution function, and finite-sample sorting is its empirical implementation. According to copula theory, monotonic transformations do not change the copula dependence structure. Since the distribution transformation is a sorting or quantile-mapping transformation, it is also a monotonic transformation.

The distribution transformation also preserves the stationarity of the original process. If $\mathbf{X}(t)$ is a stationary stochastic process, its arbitrary finite-dimensional joint distribution remains unchanged under time translation. Since the distribution transformation applies a deterministic marginal transformation to each component, the finite-dimensional joint distributions of the distribution process $\mathbf{D}(t)=[D_1(t),D_2(t),...,D_n(t)]^T$ also remain unchanged under time translation. Therefore, $\mathbf{D}(t)$ preserves the stationarity of the original process. For second-order analysis, the joint distribution of $[D_i(t)D_j(t+\tau)]$ depends only on the time lag τ.

For further normalization, the distribution process is standardized to have zero mean and unit standard deviation:

$$\overline{D}_i(t)=\sqrt{12}(D_i(t)-0.5) \tag{11}$$

The distribution correlation coefficient function after standardization is identical to that before standardization and can be written as

$$\rho_{ij}^{\text{D}}(\tau)=E(\overline{D}_i(t)\overline{D}_{\text{j}}(t+\tau)) \tag{12}$$

This function is the covariance function of the standardized distribution process. For arbitrary finite time points $t_1, t_2, ...t_m$, arbitrary components $i, j = 1, 2, ...n$, and arbitrary real coefficients $a_{i,p}$

$$\sum_{p=1}^{m}\sum_{q=1}^{m}\sum_{i=1}^{n}\sum_{j=1}^{n} a_{i,p}a_{j,q}\rho_{ij}^{\mathrm{D}}(t_q - t_p) = Var(\sum_{p=1}^{m}\sum_{i=1}^{n} a_{i,p}\overline{D}_i(t_p)) \geq 0 \tag{13}$$

Therefore, the distribution correlation coefficient matrix $\boldsymbol{\rho}^{\mathrm{D}}(\tau)$ is positive semi-definite. To obtain a covariance-equivalent representation, the distribution correlation function can be scaled by the standard deviations of the original process.

$$R_{ij}^{D}(\tau) = \sigma_i\sigma_j\rho_{ij}^{\mathrm{D}}(\tau) \tag{14}$$

Under stationarity, the distribution correlation coefficient function depends only on the time lag τ. The corresponding power spectrum can then be constructed in analogy with the Wiener–Khinchin relationship between the Pearson power spectrum and the Pearson correlation function:

$$\mathbf{R}^{D}(\tau) = \frac{1}{2\pi}\int_{-\infty}^{\infty}\mathbf{S}^{D}(\omega)e^{i\omega\tau}d\omega \tag{15}$$

$$\mathbf{S}^{D}(\omega) = \int_{-\infty}^{\infty}\mathbf{R}^{D}(\tau)e^{-i\omega\tau}d\tau \tag{16}$$

The distribution power spectrum is the power spectrum of the standardized distribution process $\overline{\mathbf{D}}(t)$ after scaling by the standard deviations. The conventional Pearson power spectrum characterizes the linear second-order structure of the original amplitude process, whereas the distribution power spectrum characterizes the frequency-domain distribution of the monotonic dependence structure. Through the distribution transformation, the influence of the marginal distribution form on the second-order dependence structure is effectively weakened.

3. Simulation procedure for non-Gaussian stochastic processes based on distribution transformation

This section presents the simulation procedure for stationary non-Gaussian stochastic processes based on distribution transformation. The objective is to generate an n-variate stationary non-Gaussian stochastic process $\mathbf{X}(t) = [X_1(t), X_2(t), ..., X_n(t)]^T$ with prescribed marginal distributions $F_i(x)$ and target second-order dependence structure. Based on the distribution transformation established above, both the standard procedure and the simplified procedure are introduced. Their applicable conditions are also discussed.

3.1 Standard simulation procedure

The standard simulation procedure based on distribution correlation is shown. The distribution structure of the target non-Gaussian process is used as an intermediate representation. The target distribution power spectrum, distribution correlation function, and underlying Gaussian correlation function are connected to construct the underlying Gaussian power spectral matrix. The target non-Gaussian process is then obtained through spectral representation and marginal transformation.

The standard procedure includes the following steps:

(1) Extract the target distribution vector process $\mathbf{R}^{\sigma}(t)$ from the target non-Gaussian process $\mathbf{X}_0(t)$.

(2) Estimate the target distribution power spectral matrix $\mathbf{S}^{D}(\omega)$.

(3) Obtain the distribution correlation matrix $\mathbf{R}^D(\tau)$ from $\mathbf{S}^D(\omega)$ through inverse Fourier transform.

(4) Transform the distribution correlation matrix $\mathbf{R}^D(\tau)$ into the underlying Gaussian correlation matrix $\mathbf{R}_U(\tau)$ using the normalized element-wise distribution transformation.

(5) Transform $\mathbf{R}_U(\tau)$ into the underlying Gaussian power spectral matrix $\mathbf{S}_U(\omega)$ through Fourier transform.

(6) Generate the underlying Gaussian process $\mathbf{U}(t)$ with the target correlation structure based on spectral representation.

(7) Apply the marginal transformation $\mathbf{X}(t) = \mathbf{T}(\mathbf{U}(t))$ to obtain the target non-Gaussian process $\mathbf{X}(t)$, which has the prescribed marginal distributions and second-order dependence structure of $\mathbf{X}_0(t)$.

The standard procedure retains the nonlinear closed-form transformation between the distribution correlation and the underlying Gaussian correlation. It is suitable for multivariate stochastic process simulation when the dependence structure is relatively complex or when high accuracy is required. However, the procedure involves repeated transformations between the frequency domain and the time domain. It also requires matrix-valued operations, spectral estimation, frequency discretization, and spectral truncation. These steps may increase the computational complexity in large-scale simulations.

3.2 Simplified simulation procedure

The standard procedure requires multiple transformations among the distribution power spectrum, distribution correlation function, underlying Gaussian correlation function, and underlying Gaussian power spectrum. To reduce the implementation complexity, the closed-form transformation between distribution correlation and the underlying Gaussian Pearson correlation can be approximated by a linear relation.

According to the previous derivation, the distribution correlation and the underlying Gaussian Pearson correlation satisfy

$$\rho_{U,ij}^{\text{Pearson}}(\tau) = 2\sin\left(\frac{\pi}{6}\rho_{ij}^{\text{D}}(\tau)\right) \tag{17}$$

Within the small-correlation range commonly encountered in engineering applications, this relation can be approximated as

$$\rho_{U,ij}^{\text{Person}}(\tau) \approx \frac{\pi}{3}\rho_{ij}^{\text{D}}(\tau) \tag{18}$$

Accordingly, the distribution power spectral matrix and the underlying Gaussian power spectral matrix can be approximately related by

$$\mathbf{S}_U(\omega) \approx \frac{\pi}{3}\mathbf{S}^D(\omega) \tag{19}$$

Figure 1 compares the standard transformation and the simplified transformation. The two curves agree well over the interval $[-1,1]$, and they are nearly identical in the small-correlation range. The approximation error increases as the distribution correlation becomes larger. Therefore, the simplified distribution transformation should be regarded as an engineering approximation rather than a strictly equivalent transformation.

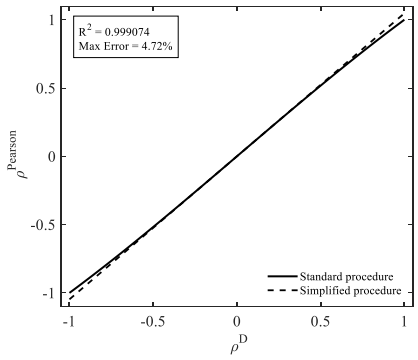

Figure 1. Comparison between the standard and simplified distribution transformations

The simplified procedure includes the following steps:

(1) Extract the target distribution vector process $\mathbf{D}^{\sigma}(t)$ from the target non-Gaussian process $\mathbf{X}_0(t)$.

(2) Estimate the target distribution power spectral matrix $\mathbf{S}^{D}(\omega)$.

(3) Obtain the underlying Gaussian power spectral matrix $\mathbf{S}_U(\omega)$ directly from $\mathbf{S}^{D}(\omega)$ using the simplified transformation

(4) Generate the underlying Gaussian process $\mathbf{U}(t)$ with the target correlation structure based on spectral representation.

(5) Apply the marginal transformation $\mathbf{X}(t)=\mathbf{T}[\mathbf{U}(t)]$ to obtain the target non-Gaussian process $\mathbf{X}(t)$.

Compared with the standard procedure, the simplified procedure has a shorter computational path and avoids repeated transformations between correlation functions and power spectral matrices. It is therefore more suitable for cases with relatively low correlation levels, fast simulation demands, or large-scale parametric analyses.

3.3 Applicability and implementation conditions

The proposed simulation method is based on the distribution process, distribution correlation, and distribution transformation. Its use requires the following theoretical and numerical conditions:

(1) Stationarity requirement. The definition of the distribution power spectrum requires the distribution correlation function to depend mainly on the time lag τ, rather than on the absolute time. Therefore, the method is applicable to stationary or approximately stationary non-Gaussian stochastic processes. If the target process contains obvious mean drift, variance modulation, abrupt regime changes, or time-varying frequency components, detrending, segmentation, or application within approximately stationary windows is required.

(2) Gaussian assumption. The method uses distribution correlation to describe monotonic dependence and converts it into the underlying Gaussian correlation structure through a closed-form relation under the Gaussian copula. Therefore, it is more suitable for non-Gaussian processes whose dependence structure can be reasonably approximated by a Gaussian copula. If the process shows significant tail dependence, asymmetric dependence, or strong non-monotonic coupling, distribution correlation alone may be insufficient to fully characterize the dependence structure.

(3) Realizability of the spectral matrix. The distribution power spectral matrix is usually estimated from finite samples. The estimate is affected by the record length, window function, overlap ratio, frequency resolution, and finite-precision ordering. In multivariate cases, estimation errors may cause the spectral matrix at some frequency points to deviate from Hermitian symmetry or positive semi-definiteness. Such deviations may affect spectral matrix decomposition and stochastic process

simulation. In engineering implementation, spectral smoothing, frequency-band truncation, Hermitian symmetrization, and negative-eigenvalue truncation can be used to improve the decomposability of the spectral matrix.

4. Numerical Examples

4.1 Single-Point Non-Gaussian Stochastic Process Example

Table 1 Parameters of five typical marginal distributions

Distribution	Parameter	Mean	Std	Skewness	Kurtosis
Normal		0	1.00	0	3.00
Lognormal	$\mu_L = 0$ $\sigma_L = 0.35$	0	1.00	1.13	5.35
Weibull	$k = 2.00$ $\lambda = 1.00$	0	1.00	0.63	3.25
Gamma	$\alpha = 3.00$ $\theta = 1.00$	0	1.00	1.15	5
Laplace	$b = 0.71$	0	1.00	0	6

This example considers five typical marginal distributions: normal, lognormal, Weibull, Gamma, and Laplace distributions. These distributions are used to represent typical non-Gaussian cases, including symmetric, right-skewed, and heavy-tailed distributions. For comparison among different distributions, all target processes are linearly standardized with zero mean and unit standard deviation. The parameters and first four statistical moments of the target marginal distributions are listed in Table 1. The target second-order structure is described by a normalized Kaimal-type one-sided power spectrum. The sampling frequency is f_s=10Hz, and the total duration is 3600 s. The Welch method is used for spectral estimation, with a Hann window, a 50% overlap ratio, and 8192 FFT points. For each distribution, a non-Gaussian stochastic process with the target marginal distribution and target power spectrum is first generated as the target process. Its distribution power spectrum is then estimated. The standard and simplified procedures are further used to generate simulated processes. Since only one sample path is generated for each distribution, this example focuses on the statistical reproduction of the marginal distribution and frequency-domain structure, rather than point-by-point agreement between time histories.

The distribution process and its distribution power spectrum are then estimated. The standard and simplified procedures are further applied to generate simulated processes. After the latent Gaussian process is generated, the same marginal mapping is used in both procedures to obtain the target non-Gaussian simulated process. Figure 2 shows the PDF comparison among the target process, the standard procedure, and the simplified procedure for the five marginal distributions. Overall, the three curves show good agreement in the main distribution region, indicating that both procedures can recover the target marginal distribution well. For the Laplace distribution, slight deviations appear near the peak and tail regions because of its sharper peak and heavier tail. Nevertheless, the overall distribution shape is still preserved.

Figure 3 shows the power spectral density comparison among the target process and the two simulated processes for the five marginal distributions. The three curves show similar spectral shapes and decay trends in the dominant energy frequency range, indicating that the target second-order frequency-domain structure is effectively reproduced. The local fluctuations in the high-frequency range are mainly related to finite-sample spectral estimation based on a single sample path.

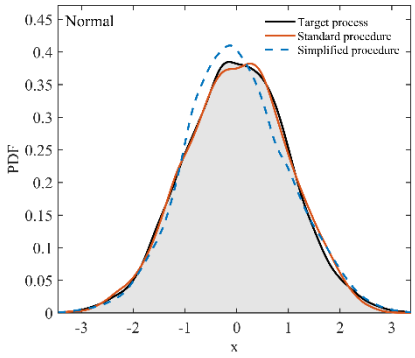

(a) Normal

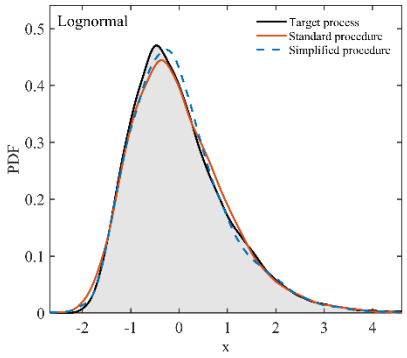

(b) Lognormal

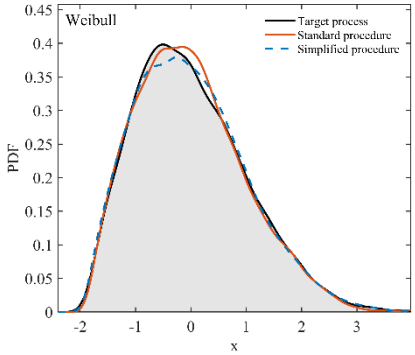

(c) Weibull

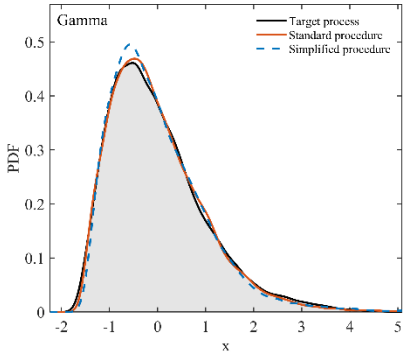

(d) Gamma

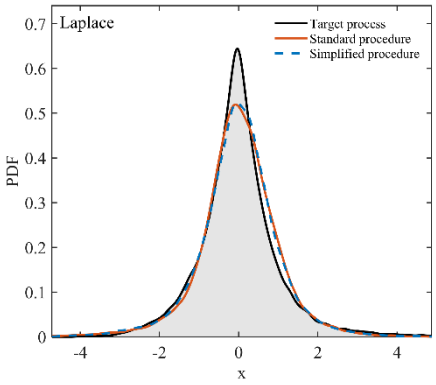

(e) Laplace

Figure 2: PDF comparison under five typical marginal distributions

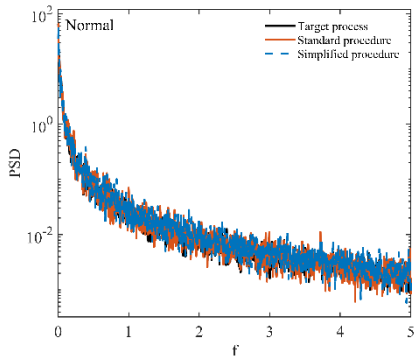

(a) Normal

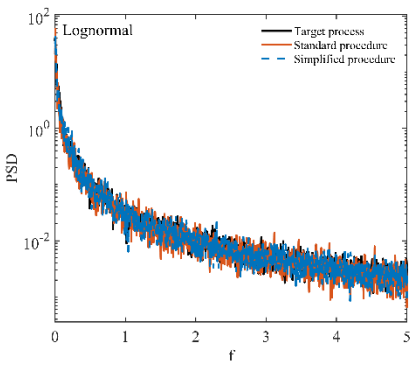

(b) Lognormal

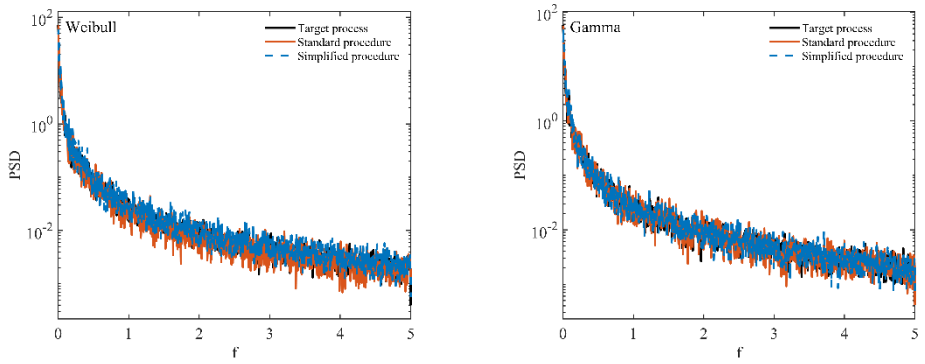

(c) Weibull

(d) Gamma

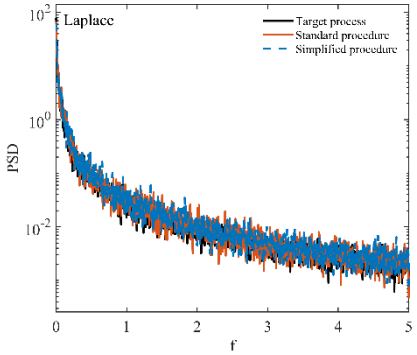

(e) Laplace

Figure 3: PSD comparison under five typical marginal distributions

To further quantify the reproduction of marginal distributions, the K-S distance is used to evaluate the maximum deviation between the empirical distribution functions of the target and simulated processes. It is defined as

$$D_{KS} = \sup\left|F_X(x) - F_Y(x)\right| \tag{20}$$

where $F_X(x)$ and $F_Y(x)$ are the empirical distribution functions of the target process and the simulated process, respectively. The log-spectral error is also used to evaluate the difference between the target spectrum and the simulated spectrum:

$$\varepsilon_{\log} = \sqrt{\frac{1}{K}\sum_{f_k \in \mathbf{B}} [\log_{10} S_1(f_k) - \log_{10} S_2(f_k)]^2} \tag{21}$$

where B is the evaluation frequency band, K is the number of frequency points in this band, and $S_1(f_k)$ and $S_2(f_k)$ are the two power spectra to be compared.

Table 2: Comparison of simulation error parameters for the two procedures

Distribution	Standard procedure		Simplified procedure	
	D_{KS}	$\varepsilon_{\log}$	D_{KS}	$\varepsilon_{\log}$
Normal	0.008	0.127	0.024	0.146
Lognormal	0.016	0.149	0.016	0.139
Weibull	0.010	0.149	0.011	0.143
Gamma	0.009	0.142	0.017	0.136
Laplace	0.050	0.158	0.051	0.177

Table 2 summarizes the main error indices for the single-point example. Except for the Laplace case, the K-S distances remain below 0.02 for both procedures. The larger K-S distance for the Laplace distribution is mainly caused by the higher sensitivity of its sharp peak and heavy tail to finite-sample errors. The log-spectral errors of the two procedures are of the same order of magnitude, indicating that the simplified procedure does not significantly weaken the reproduction capability for the main frequency-domain structure, although it adopts a linear approximation.

4.2 Two-Dimensional Multi-Point Inflow Wind Field Example

To further verify the applicability of the proposed method to multi-point stochastic process simulation, a two-dimensional cross-sectional stationary non-Gaussian inflow wind field is constructed. This example does not repeat the discussion on the recovery of single-point marginal distributions and auto-power spectra. Instead, it focuses on the preservation of cross-power spectra and frequency-domain coherence structures under multi-point conditions.

The two-dimensional inflow section adopts a 7×7regular grid with 49 measurement points, as shown in Figure 4. The central point is denoted as $(0, 0)$, with a height of 90 m. The horizontal and vertical spacings between adjacent points are both 20 m. Thus, the seven height levels are 30, 50, 70, 90, 110, 130, and 150 m. A 1 h wind speed process is generated at each measurement point, with a sampling frequency of 10 Hz. The whole wind field sample can therefore be regarded as a 49-dimensional stationary non-Gaussian random vector process.

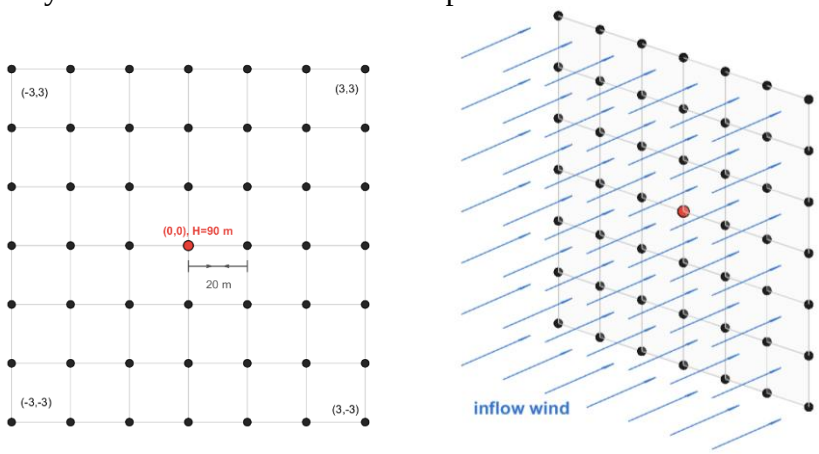

(a) Layout of measurement points (b) Inflow wind field schematic

Figure 4: Schematic of the inflow wind field and measurement point layout

The target marginal distribution at each height level is described by the Johnson $S_U$distribution to represent mild right-skewness and peak-heavy-tail characteristics of wind speed fluctuations. The target mean is determined by the standard wind speed profile, and the standard deviation varies with height. The target marginal statistical parameters at the seven height levels are listed in Table 3.

Table 3: Target marginal statistical characteristics of the seven height level

Height H(m)	Mean(m/s)	Std(m/s)	Skewness	Kurtosis
30	23.84	3.57	0.284	4.360
50	25.87	3.88	0.263	4.057
70	27.30	4.09	0.272	4.069
90	28.42	4.26	0.214	3.959
110	29.35	4.40	0.189	4.158
130	30.14	4.52	0.207	3.862
150	30.84	4.62	0.185	3.863

The target second-order structure is determined jointly by the single-point auto-power spectrum and the point-to-point coherence function. The auto-power spectrum at each point is described by the Kaimal spectrum, and the spatial coherence between measurement points is described by the Davenport exponential coherence model:

$$\gamma_{ij}(f) = \exp(-C\frac{fd_{ij}}{\overline{U}_{ij}}) \tag{22}$$

where d_{ij} is the spatial distance between two measurement points, $\bar{U}_{ij}$ is the average mean wind speed of the two points, and C is the coherence decay coefficient. The cross-power spectrum between any two measurement points is then constructed as

$$S_{ij}(f) = \gamma_{ij}(f)\sqrt{S_{ii}(f)S_{jj}(f)} \tag{23}$$

In this way, the target power spectral matrix of the 49-point two-dimensional inflow wind field is obtained. After the target process is generated, the standard and simplified procedures are applied for simulation. The preservation of the multi-point spatial correlation structure is then evaluated from the cross-power spectrum and coherence matrix.

Figure 5 shows the cross-power spectrum comparison for six representative measurement point pairs. The cross-power spectrum reflects the frequency-domain spatial correlation between different measurement points. It can therefore be used to examine the reproduction of the spatial coupling structure of the multi-point wind field. The results show that both procedures can follow the variation trend of the target cross-power spectra in the low-frequency range, indicating that the main spatial correlation structure is preserved. As frequency increases, the fluctuations of the cross-power spectral curves become stronger, and the differences between the simulated and target results increase. This is mainly related to finite-sample spectral estimation and the higher difficulty of recovering multi-point correlation structures.

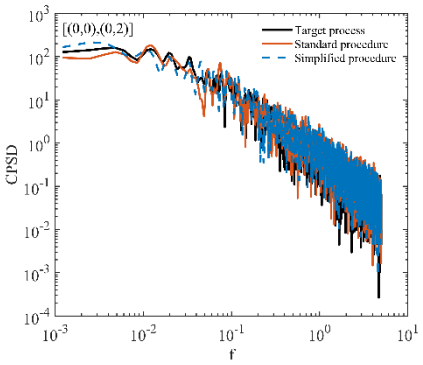

(a) [(0,0),(0,2)]

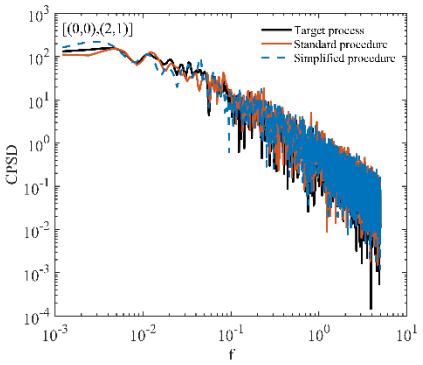

(b) [(0,0),(2,1)]

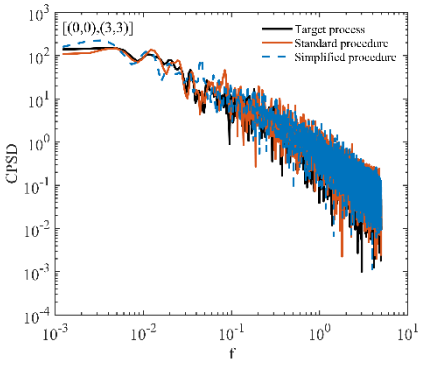

(c) [(0,0),(3,3)]

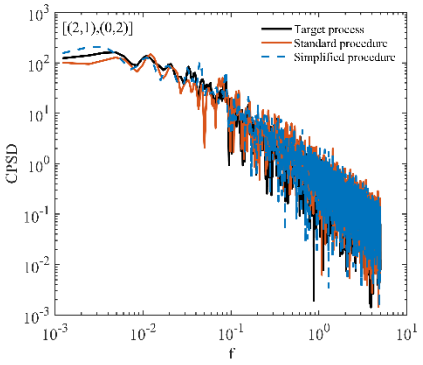

(d) [(0,2),(2,1)]

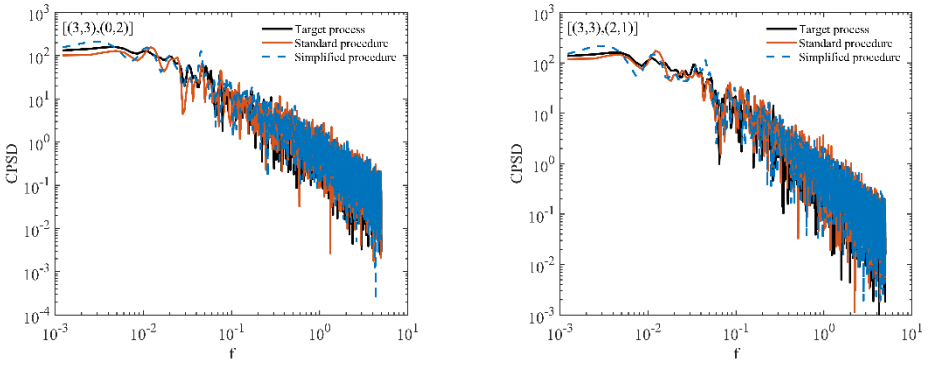

(e) [(0,2),(3,3)] (f) [(2,1),(3,3)]

Figure 5: Cross-PSD comparison for six representative measurement point pairs

Table 4 lists the cross-power spectral errors of the six representative measurement point pairs in the low-frequency and mid-low-frequency bands. Overall, both procedures maintain relatively small errors in the low-frequency range, indicating that the spatial correlation characteristics in the dominant energy range are well reproduced. Compared with the auto-power spectrum, the cross-power spectral errors are relatively larger, showing that the recovery of multi-point spatial coupling structures is more difficult than that of single-point frequency-domain structures.

Table 4: Comparison of CPSD errors for six representative grid-point pairs

Grid point pair	Standard procedure		Simplified procedure	
	$\varepsilon_{\log}(f<0.2\text{Hz})$	$\varepsilon_{\log}(f<0.5\text{Hz})$	$\varepsilon_{\log}(f<0.2\text{Hz})$	$\varepsilon_{\log}(f<0.5\text{Hz})$
[(0,0),(0,2)]	6.36%	11.6%	7.08%	13.3%
[(0,0),(2,1)]	9.63%	16.1%	8.25%	16.8%
[(0,0),(3,3)]	9.97%	22.1%	8.09%	20.4%
[(0,2),(2,1)]	8.40%	23.9%	6.34%	17.2%
[(0,2),(3,3)]	5.79%	19.5%	7.25%	19.7%
[(2,1),(3,3)]	7.57%	15.5%	4.52%	13.9%

To further examine the frequency-domain spatial correlation structure at the matrix level, Figure 6 shows the coherence matrix heatmap at the representative frequency f=0.1Hz. The target coherence matrix presents a clear main diagonal band. The high-value region is mainly distributed near the main diagonal, indicating that measurement points with shorter spatial distances have stronger coherence. Both the standard and simplified procedures can recover this overall spatial distribution pattern, indicating that both procedures can preserve the main frequency-domain coherence structure of the two-dimensional wind field. In comparison, the standard procedure is closer to the target result in the continuity of the high-value region. The simplified procedure shows more local fluctuations, but it still preserves the main diagonal band and the overall spatial decay pattern.

Overall, the single-point example and the two-dimensional multi-point inflow wind field example show that the proposed non-Gaussian stochastic process simulation method based on distribution power spectra can effectively recover the target second-order dependence structure while preserving the target marginal distribution. The standard procedure is more stable in recovering multi-point spatial correlation structures. The simplified procedure reduces the implementation complexity while still preserving the main statistical characteristics, making it suitable for rapid simulation and large-scale parametric analysis.

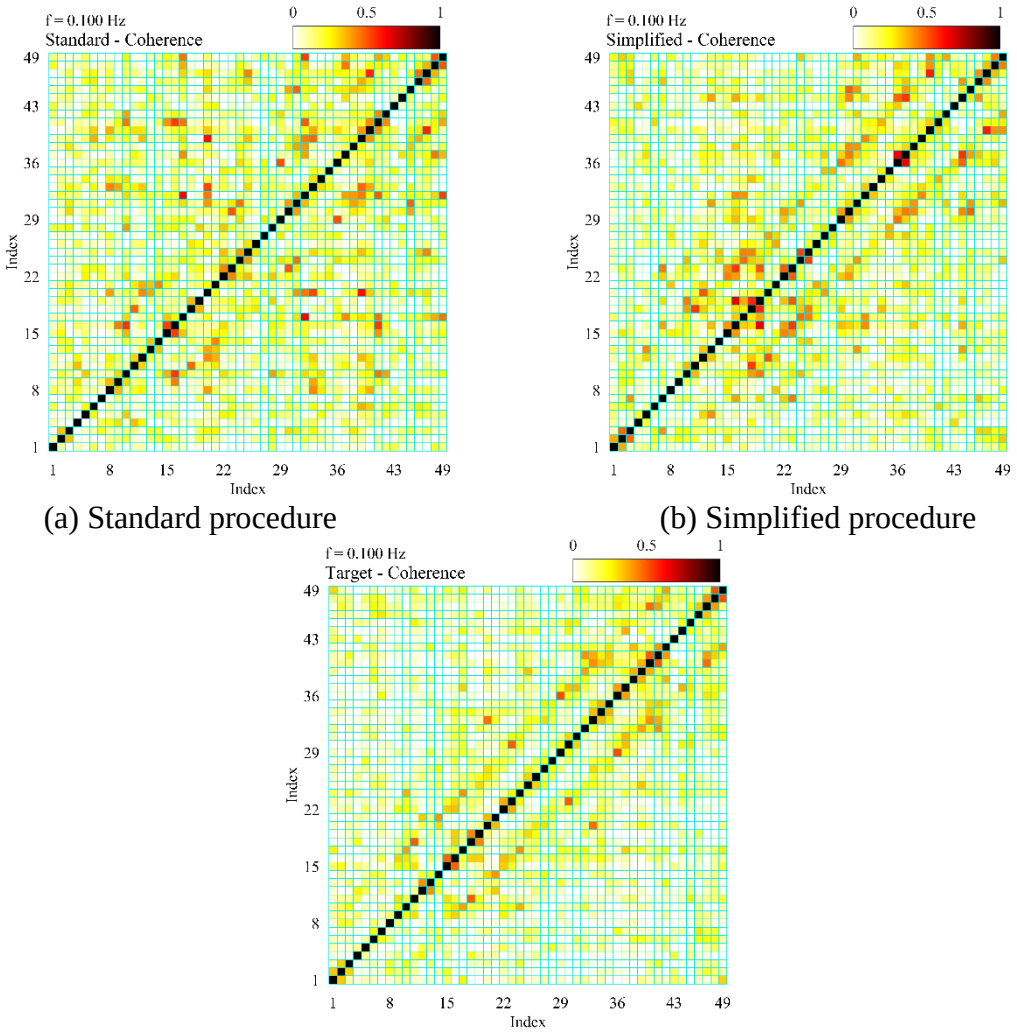

(a) Standard procedure (b) Simplified procedure

(c) Target process

Figure 6: Coherence heatmap at the representative frequency of 0.1 Hz

5. Conclusion

This study developed a distribution transformation-based method for simulating stationary non-Gaussian stochastic processes. By establishing the distribution process as an intermediate representation, the marginal distribution and the distribution-based dependence structure can be specified in a more coordinated manner. A standard procedure and a simplified procedure were developed to construct the underlying Gaussian spectral structure and then generate the target non-Gaussian process through marginal transformation.

The main findings are summarized as follows. First, the distribution power spectrum provides an effective frequency-domain representation of the dependence structure of non-Gaussian stochastic processes. Second, the single-point example shows that both procedures can reproduce the target marginal distributions and the main PSD characteristics. Third, the multi-point inflow wind field example shows that the proposed method can reasonably preserve cross-PSD and coherence structures. The standard procedure gives more stable results for multi-point dependence, whereas the simplified procedure retains the main statistical characteristics with lower implementation complexity, making it suitable for rapid simulation and large-scale parametric analysis.

References

[1] Rice SO. Mathematical analysis of random noise. Bell Syst Tech J 1944;23(3):282–332.
[2] Borgman LE. Ocean wave simulation for engineering design. J Waterw Harbors Div 1969;95(4):557–583.
[3] Shinozuka M. Monte Carlo solution of structural dynamics. Comput Struct 1972;2(5–6):855–874.
[4] Shinozuka M, Jan CM. Digital simulation of random processes and its applications. J Sound Vib 1972;25(1):111–128.
[5] Yang JN. Simulation of random envelope processes. J Sound Vib 1972;21(1):73–85.
[6] Yang JN. On the normality and accuracy of simulated random processes. J Sound Vib 1973;26(3):417–428.
[7] Shields D M, Kim H. Simulation of higher-order stochastic processes by spectral representation[J]. Probabilistic Engineering Mechanics,2017,1-15. DOI:10.1016/j.probengmech.2016.11.001.
[8] Deodatis G, Shields M. The spectral representation method: A framework for simulation of stochastic processes, fields, and waves. Reliab Eng Syst Saf 2025;254:110522.
[9] Deodatis G. Simulation of ergodic multivariate stochastic processes. J Eng Mech 1996;122(8):778–787.
[10] Li Y, Kareem A. Simulation of multivariate random processes: Hybrid DFT and digital filtering approach. J Eng Mech 1993;119(5):1078–1098.
[11] Johnson NL. Systems of frequency curves generated by methods of translation. Biometrika 1949;36(1/2):149–176.
[12] Grigoriu M. Crossings of non-Gaussian translation processes. J Eng Mech 1984;110(4):610–620.
[13] Gurley KR, Kareem A, Tognarelli MA. Simulation of a class of non-normal random processes. Int J Non-Linear Mech 1996;31(5):601–617.
[14] Puig B, Poirion F, Soize C. Non-Gaussian simulation using Hermite polynomial expansion: Convergences and algorithms. Probab Eng Mech 2002;17(3):253–264.
[15] Sakamoto S, Ghanem R. Polynomial chaos decomposition for the simulation of non-Gaussian nonstationary stochastic processes. J Eng Mech 2002;128(2):190–201.
[16] Li J, Li C. Simulation of non-Gaussian stochastic process with target power spectral density and lower-order moments. J Eng Mech 2012;138(5):391–404.
[17] Ma X, Xu F. An efficient simulation algorithm for non-Gaussian stochastic processes. J Wind Eng Ind Aerodyn 2019;194:103984.
[18] Lu ZH, Zhao Z, Zhang XY, et al. Simulating stationary non-Gaussian processes based on unified Hermite polynomial model. J Eng Mech 2020;146(7):04020067.
[19] Zhao YG, Wang T, Ji X, et al. Quartic Hermite polynomial model-based translation method for extreme wind load estimation. J Wind Eng Ind Aerodyn 2024;245:105653.
[20] Wise G, Traganitis A, Thomas J. The effect of a memoryless nonlinearity on the spectrum of a random process. IEEE Trans Inf Theory 2003;23(1):84–89.
[21] Zheng R, Guoping C, Huaihai C. Stationary non-Gaussian random vibration control: A review. Chin J Aeronaut 2021;34(1):350–363.
[22] Yamazaki F, Shinozuka M. Digital generation of non-Gaussian stochastic fields. J Eng Mech 1988;114(7):1183–1197.
[23] Deodatis G, Micaletti RC. Simulation of highly skewed non-Gaussian stochastic processes. J Eng Mech 2001;127(12):1284–1295.
[24] Shields MD, Deodatis G, Bocchini P. A simple and efficient methodology to approximate a general non-Gaussian stationary stochastic process by a translation process. Probab Eng Mech 2011;26(4):511–519.
[25] Shields M, Deodatis G. A simple and efficient methodology to approximate a general non-Gaussian stationary stochastic vector process by a translation process with applications in wind velocity simulation. Probab Eng Mech 2013;31:19–29.
[26] Bocchini P, Deodatis G. Critical review and latest developments of a class of simulation algorithms for strongly non-Gaussian random fields. Probab Eng Mech 2008;23(4):393–407.
[27] Grigoriu M. Existence and construction of translation models for stationary non-Gaussian processes. Probab Eng Mech 2009;24(4):545–551.
[28] Seong SH, Peterka JA. Digital generation of non-Gaussian spiky excitations using spectral representation with additive phase structure. J Eng Mech 2012;138(10):1236–1248.
[29] Steinwolf A. Random vibration testing with kurtosis control by IFFT phase manipulation. Mech Syst Signal Process 2012;28:561–573.
[30] Shields MD, Kim H. Simulation of higher-order stochastic processes by spectral representation. Probab Eng Mech 2017;47:1–15.
[31] Vandanapu L, Shields MD. 3rd-order spectral representation method: Simulation of multi-dimensional random fields and ergodic multi-variate random processes with fast Fourier transform implementation. Probab Eng Mech 2021;64:103128.
[32] Sklar A .Fonctions de Repartition a n Dimensions et Leurs Marges[J].Publ.inst.statist.univ.paris, 1959.

[33] Liu PL, Der Kiureghian A. Multivariate distribution models with prescribed marginals and covariances. Probab Eng Mech 1986;1(2):105–112.
[34] Rosenblatt M. Remarks on a multivariate transformation. Ann Math Stat 1952;23(3):470–472.
[35] Genest C, Favre AC. Everything you always wanted to know about copula modeling but were afraid to ask. J Hydrol Eng 2007;12(4):347–368.
[36] Lebrun R, Dutfoy A. An innovating analysis of the Nataf transformation from the copula viewpoint. Probab Eng Mech 2009;24(3):312–320.
[37] Nelsen RB. An Introduction to Copulas. Springer; 2006.
[38] Joe H. Dependence Modeling with Copulas. CRC Press; 2014.
[39] C S. The proof and measurement of association between two things [J]. International journal of epidemiology, 2010,39(5):1137-50. DOI:10.1093/ije/dyq191.
[40] Kendall MG. A new measure of rank correlation. Biometrika 1938;30(1–2):81–93.
[41] Iman RL, Conover WJ. A distribution-free approach to inducing rank correlation among input variables. Commun Stat Simul Comput 1982;11(3):311–334.